Mapping T Cell Antitumor Responses in Whole Blood to Solid Tumor Tissue Biopsies of Cancer Patients with Mass Cytometry

Ling Wang, Qanber Raza, Nick Zabinyakov, Lauren Tracey, Michael Cohen, Stephen Li, Nikesh Parsotam, David Howell, Liang Lim, Christina Loh

CYTO 2025

Introduction

Over the last decade, immunotherapy has revolutionized cancer treatment, yet it exhibits limited efficacy in treating solid tumors. The main challenges include T cell exhaustion, an immunosuppressive tumor microenvironment (TME), a lack of tumor-specific antigens and a complex immune landscape. Recent studies indicate that solid tumors induce dramatic changes in the systemic immune system that are highly dynamic over the course of tumor progression. To overcome the limitation of current immunotherapies and develop safe and effective novel immunotherapies, it is crucial to achieve a comprehensive understanding of the localized and systemic immune responses.

Here, we took an integrative approach of mapping localized and systemic immune cell responses by employing CyTOF™ and Imaging Mass Cytometry™ (IMC™) technology in matched peripheral blood mononuclear cells (PBMC), tumor-derived cells (TDC) and formalin-fixed, paraffin-embedded (FFPE) tumor tissues from clear cell renal cell carcinoma (ccRCC) patients.

CyTOF analysis on PBMC and TDC revealed phenotypic and functional heterogeneity, including T cell exhaustion and activation profiles and dysregulated macrophage phenotypes. The IMC approach further elucidated the spatial relationships of immune subsets relative to tumor cells, vasculature and stromal components, uncovering distinct patterns of immune infiltration and congregation. Comparison of CyTOF and IMC data revealed shared and divergent phenotypes between peripheral and tissue-resident immune compartments, highlighting potential biomarkers linking systemic immune profiles and the spatial heterogeneity of the TME.

Materials and methods

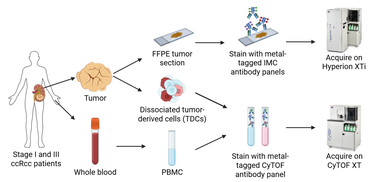

Figure 1. Workflow overview. Tumor tissue and whole blood from one Stage 1 and one Stage 3 ccRCC patient were obtained. Tumor tissue was processed in two ways: (1) FFPE tumor sections were stained with IMC antibody panels and acquired on a Hyperion™ XTi Imaging System; (2) tumor cells were enzymatically digested into dissociated TDC. PBMC derived from the patient whole blood sample and TDC were stained with a CyTOF antibody panel and analyzed on a CyTOF XT system.

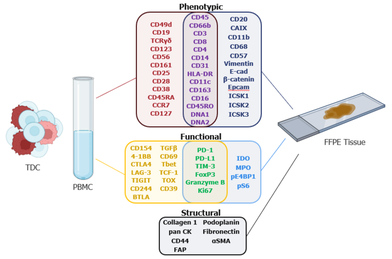

Figure 2. Antibody panels used in this study. TDC and PBMC samples were stained with a CyTOF panel, depicted in the dark blue, light blue and **black** bubbles. Bubble overlap indicates shared markers between the CyTOF and IMC panels. See QR code at the bottom of the poster for additional details and ordering information.

Key takeaways

- The **integrated approach** demonstrates the power of mass cytometry for comprehensive **functional profiling** of T cells and their **spatial organization**. These findings provide a foundation for understanding the immunological crosstalk between the peripheral immune system and the tumor microenvironment (TME) driving antitumor responses.

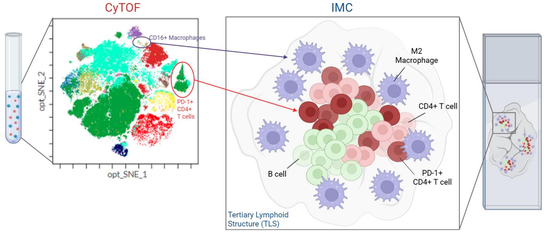

- Deep **single-cell profiling** using a **high-parameter CyTOF panel** unveiled an **immunosuppressive TME** composed of exhausted T and NK cells and suppressed macrophages in ccRCC patients
- **In-depth T cell profiling** revealed enriched naive and cytotoxic phenotypes in PBMC, while **exhausted** TEM and TCM cells with impaired cytotoxicity dominate in TME, along with an increased **Treg** population
- **A comprehensive IMC panel** revealed **heterogeneous cell composition** in TME
- **Tertiary lymphoid structures** were identified in the TME and harbored exhausted CD4+ T cells. Surrounding M2 macrophages indicate significant contribution to T cell exhaustion phenotype identified by CyTOF.

Results

Deep functional profiling with CyTOF technology reveals an immunosuppressive TME

Population frequencies visualized in high-dimensional space differ across cell types and between patients

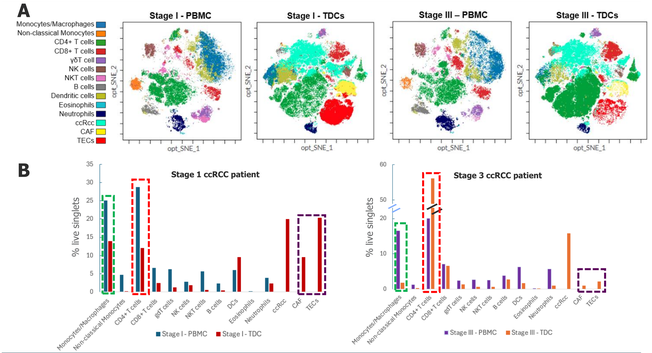

Exhausted T and NK cells, along with suppressive macrophages, were found in TME

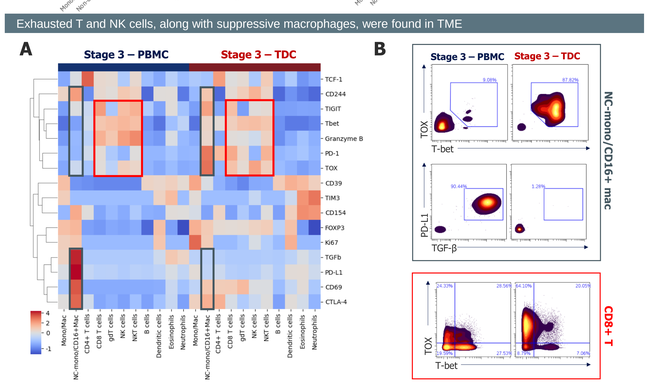

In-depth profiling revealed exhaustive phenotype of T cells within the TME with an increased Treg population

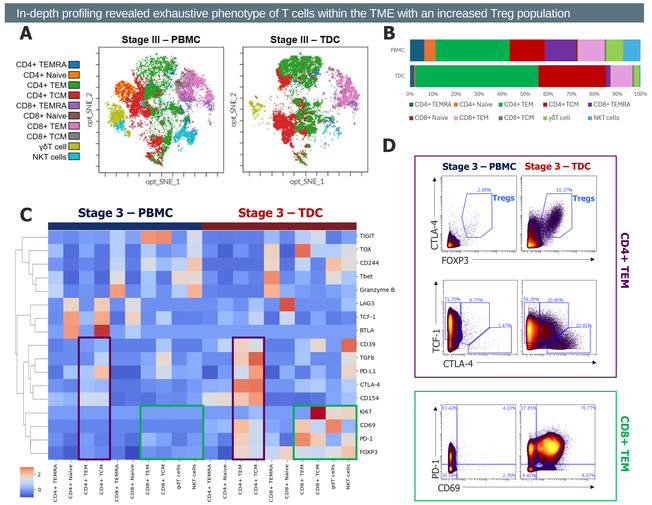

Figure 3. Cell composition differs between PBMC and TDC samples in Stage 1 and 3 ccRCC patients.

(A) opt-SNE, a dimensionality reduction tool, was applied to live singlet cells from either PBMC samples or TDC samples and plotted. Overlaid colors correspond to gated cell populations. 73,000 events (PBMC) or 200,000 events (TDC) were proportionally sampled across two patients. Clear discrimination of major cell populations is observed.

(B) Quantification of gated cells subsets shown in Figure 3A represented as a percentage of total live singlets.

Proportions of monocytes/macrophages are substantially decreased in TDC compared with PBMC for both patients (green box); the difference is >seven-fold for the Stage 3 patient.

The proportion of CD4+ T cells is 2.8-fold higher in TDC of the Stage 3 patient compared with PBMC (red box) at the expense of monocytes/macrophages, cancer-associated fibroblasts (CAF) and tumor-associated endothelial cells (TEC; purple box).

Figure 4. Exhaustion and effector phenotypes were observed in T, NK and myeloid cell subsets in Stage 3 ccRCC.

(A) Heat map of median signal intensity for each functional marker (Y-axis) across major cell populations (X-axis) in Stage 3 patient PBMC (left, blue bar) and TDC (right, red bar). Scale bar shows median intensity Z score normalized within each marker.

(B) Biaxial plots from non-classical (NC) monocytes/CD16+ macrophage subset (grey box) or CD8+ T cells (red box).

Non-classical monocytes appear highly functional in PBMC, expressing PD-L1 and TGF-β, however, differentiated macrophages in the TME become dysfunctional and suppressed, expressing TOX and T-bet.

T cells and NK cells exhibited an exhausted phenotype, particularly in TDC (less effector cytokine and upregulated PD-1/TOX).

Figure 5. Profiling of systemic and local T cell subsets reveals differences in functional phenotypes in Stage 3 patient.

(A) opt-SNE was applied to CD3+ cells from either PBMC samples or TDC samples from the Stage 3 patient and plotted. Overlaid colors correspond to gated cell populations. 30,000 events were proportionally sampled across the two samples. Clear discrimination of major T cell populations is observed.

(B) Stacked bar chart quantifying the proportion of each cell subset within CD3+ T cells.

Very few naive T cells are found in TDC, whereas a large increase in CD4+ TEM and TCM cells is observed compared with PBMC.

(C) Heat map of median signal intensity for each functional marker (Y-axis) across T cell subsets (X-axis) in Stage 3 patient PBMC (left, blue bar) and TDC (right, red bar). Scale bar shows median intensity Z score normalized within each marker.

(D) Biaxial plots from CD4+ TEM (purple box) or CD8+ TEM (green box) cell subsets.

Overall, naive/memory phenotypes are seen PBMC, with higher TCF-1 expression in naive and TCM T cell subsets and a more cytotoxic phenotype in CD8+ TEMRA (granzyme B+), whereas higher expression of exhaustion markers is observed in the TME in CD4 TEM/TCM subsets (for example, PD-1, CTLA-4, TOX). Within the CD4+ TEM subset, an increase in FoxP3+ Treg population was observed. Exhausted CD8+ TEM cells are found exclusively in TDC (CD69+PD-1+).

IMC image highlights spatial distribution of functional immune cells identified by CyTOF technology

Pixel-clustering analysis of Tissue Mode images spatially resolves major phenotypic clusters, including immune cells, tumor cells, stroma and TLS-like structures

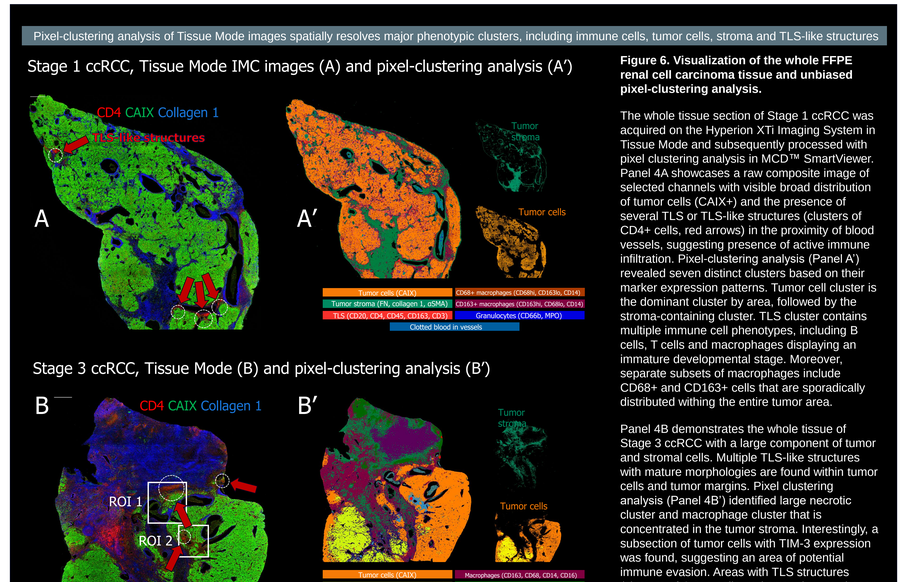

Figure 6. Visualization of the whole FFPE renal cell carcinoma tissue and unbiased pixel-clustering analysis.

The whole tissue section of Stage 1 ccRCC was acquired on the Hyperion XTi Imaging System in Tissue Mode and subsequently processed with pixel clustering analysis in MCD™ SmartViewer. Panel 4A showcases a raw composite image of selected channels with visible broad distribution of tumor cells (CAIX+) and the presence of several TLS or TLS-like structures (clusters of CD4+ cells, red arrows) in the proximity of blood vessels, suggesting presence of active immune infiltration. Pixel-clustering analysis (Panel A') revealed seven distinct clusters based on their marker expression patterns. Tumor cell cluster is the dominant cluster by area, followed by the stroma-containing cluster. TLS cluster contains multiple immune cell phenotypes, including B cells, T cells and macrophages displaying an immature developmental stage. Moreover, separate subsets of macrophages include CD68+ and CD163+ cells that are sporadically distributed withing the entire tumor area.

Panel 4B demonstrates the whole tissue of Stage 3 ccRCC with a large component of tumor and stromal cells. Multiple TLS-like structures with mature morphologies are found within tumor cells and tumor margins. Pixel clustering analysis (Panel 4B') identified large necrotic cluster and macrophage cluster that is concentrated in the tumor stroma. Interestingly, a subsection of tumor cells with TIM-3 expression was found, suggesting an area of potential immune evasion. Areas with TLS structures (clusters of CD4+ cells, red arrows) were chosen for further investigation in Cell Mode and single-cell segmentation analysis (see figures below). Scale bar in Panels A and B is 1 mm.

Single-cell segmentation analysis of Cell Mode images reveals a crucial role of M2 macrophages in T cell exhaustion

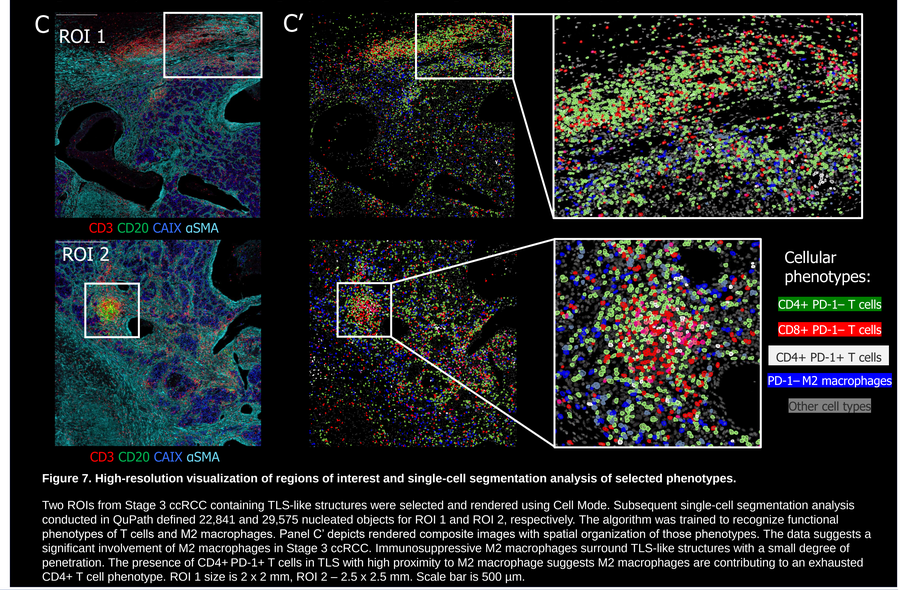

Figure 7. High-resolution visualization of regions of interest and single-cell segmentation analysis of selected phenotypes.

Two ROIs from Stage 3 ccRCC containing TLS-like structures were selected and rendered using Cell Mode. Subsequent single-cell segmentation analysis conducted in QuPath defined 22,841 and 29,575 nucleated objects for ROI 1 and ROI 2, respectively. The algorithm was trained to recognize functional phenotypes of T cells and M2 macrophages. Panel C' depicts rendered composite images with spatial organization of those phenotypes. The data suggests a significant involvement of M2 macrophages in Stage 3 ccRCC. Immunosuppressive M2 macrophages surround TLS-like structures with a small degree of penetration. The presence of CD4+ PD-1+ T cells in TLS with high proximity to M2 macrophage suggests M2 macrophages are contributing to an exhausted CD4+ T cell phenotype. ROI 1 size is 2 x 2 mm, ROI 2 – 2.5 x 2.5 mm. Scale bar is 500 µm.

Standard BioTools Inc.
2 Tower Place, Suite 2000, South San Francisco, CA 94080 USA
+1 650 266 6000 • Toll-free in the US and Canada: 866 359 4354
standardbio.com

Full panel and purchase list

Download this poster